Characterization and Evaluation of Pre-clinical Suitability of a Syngeneic Orthotopic Mouse Ovarian Cancer Model

SUNGPIL CHO[1], YONGEN SUN[1], ANDREW P. SOISSON[1], MARK K. DODSON[1], C. MATTHEW PETERSON[1], ELKE A. JARBOE[2], ANNE M. KENNEDY[3] and MARGIT M. JANÁT-AMSBURY[1,4]

[1]Division of Gynecologic Oncology, Department of Obstetrics and Gynecology, and [2]Pathology, [3]Radiology, and [4]Pharmaceutics and Pharmaceutical Chemistry, University of Utah, Salt Lake City, UT, U.S.A.

Abstract. *Background/Aim: To develop and characterize the pre-clinical suitability of a syngeneic mouse epithelial ovarian cancer model in immunocompetent hosts. Materials and Methods: ID8 mouse ovarian surface epithelium cells were implanted into the left ovarian bursa of C57BL/6 mice. Using conventional as well as ultrasound-based techniques and histopathological analysis, the tumor weights, volumes, metastases, ascites and vascularity were observed over a period of 16 weeks. Results: Ovarian weights and volume increased 12- and 7-fold, respectively. Ultrasound measurements of ovarian ID8 tumors correlated with the actual size obtained following surgical excision. Ascites and metastasis were first observed at 12 weeks post-orthotopic implantation. Histopathological analysis indicated similarities between orthotopically-generated ovarian tumors and human ovarian tumors. However, there was less evidence of angiogenesis in this animal model. Conclusion: The development of this mouse model closely replicates characteristics seen in human ovarian cancer with feasibility of using ultrasound to assess tumor formation, progression and vascularization.*

Ovarian cancer is the second most frequent invasive malignancy of female reproductive cancer and the most common cause of death among women with gynecological malignancies, with an estimated 22,280 cases diagnosed and 15,500 deaths annually in the U.S. alone (1). Epithelial ovarian cancer (EOC) accounts for over 90% of all ovarian malignancies, still related to high mortality despite advances in treatment regimens, with overall 5-year survival rates of only 46% and even lower rates (28%) for patients with metastatic disease (2, 3). Considering that most EOCs are diagnosed at an advanced stage with the tumor being widely metastatic the development of appropriate disease models, more precisely recapitulating tumorigenesis during early to advanced stages has an immediate demand (4).

Small animal (primarily mouse) EOC models are currently created in various ways: xenografting, genetic engineering or carcinogen exposure. Xenografting involves the subcutaneous (*s.c.*), intraperitoneal (*i.p.*) or orthotopic injection of single-cell suspensions of human EOC cells into immunecompromised mice (5). Xenograft models have shown some features of human EOC, such as primary tumor progression, ascites, and metastatic spread within the peritoneal cavity (5, 6). In addition to the lack of an intact immune system, a known important mediator of cancer progression and metastasis, the xenograft approach cannot comprehensively address the importance of the tumor microenvironment, showing selective advantages when cells are injected into anatomically different tissues or organs, such as subcutaneous injections of ovarian cancer cells (5, 6). Genetically-engineered mice that develop spontaneous tumors include transgenic models, a genetically induced EOC model designed to allow the development of EOC in immune competent animals (7). Connolly *et al*. developed an EOC model with a genetic construct of Simian virus 40 T-antigen (SV40 TAg) under the control of the Mullerian inhibitory substance type II receptor (MISIIR) gene promoter and obtained bilateral ovarian tumors in only 50% (8). However, the genetic contribution of SV40 TAg to ovarian carcinogenesis remains an unanswered question (4) and the lack of understanding of EOC-specific promoters makes it difficult to create a genetically-engineered mouse model (5). Carcinogen induced tumor models unfortunately only yield extremely low incidence ratios (3%) (9), develop non-organ specific tumors (10), and do not clearly associate induced

Correspondence to: Margit M. Janát-Amsbury, Division of Gynecologic Oncology, Department of Obstetrics and Gynecology, University of Utah, Salt Lake City, UT 84132, U.S.A. Tel: +1 8012132248, Fax: +1 8015859295, e-mail: margit.janat-amsbury@hsc.utah.edu

Key Words: Human epithelial ovarian cancer, EOC, mouse ovarian surface epithelium, MOSE, orthotopic ovarian cancer, immuno-competent C57BL/6.

tumors with ovarian cancer etiology (11). By using these animal models, outcomes from pre-clinical and clinical trials remain to correlate poorly.

In addition to a previous report of a syngeneic, orthotopic animal model of EOC (5, 6), we further addressed details of tumorigenesis, progression and metastatic spread in this model. We also successfully confirmed the application of conventional ultrasound imaging techniques for the precise and reproducible monitoring of tumorigenesis and progression *in vivo*.

Materials and Methods

Cell culture and animals. ID8 cells were generously provided by Dr. G. Coukos (University of Pennsylvania, USA) (12). ID8 is a cell line derived from C57BL/6 mouse ovarian surface epithelial cells, which underwent spontaneous malignant transformation in vitro (12). The cells were maintained in Dulbecco's Modified Eagle's Medium (DMEM; Invitrogen, Carlsbad, CA, USA) supplemented with 4% fetal bovine serum (Denville, Metuchen, NJ, USA), 1% penicillin/streptomycin solution (Invitrogen), and 1% insulin-transferrin-selenium-X Supplement (Invitrogen) in an incubator with a humidified atmosphere with 5% CO_2 at 37˚C. C57BL/6 mice were obtained from Jackson Laboratories (Bar Harbour, ME, USA) and housed under standard conditions in the Center for Comparative Medicine Animal Facility under the guidelines of the Institutional Animal Care and Use Committee (IACUC) at the University of Utah.

In vivo tumor generation and measurement. Six-to 8-week-old, female C57BL/6 mice were anesthetized with isofluorane and a single dorsal midline incision allowed access to both ovaries. ID8 cells (1.0×10^6) were then injected into the left ovarian bursa. The contralateral ovary was injected with equivalent amounts of PBS serving as surgical control. Animals were monitored daily and weighed twice a week. At pre-defined time points, animals (n=5) were euthanized and tumors were surgically harvested. Tumor size and weight were captured with digital calipers (Traceable Digital Carbon Fiber Calipers, Fisher Scientific, Pittsburgh, PA, USA) and a microbalance (AG104, Mettler Toledo, Columbus, OH, USA). Tumor volumes were calculated as $V=½\ (L\times W)^2$, L being the tumor length (longest dimension) and W the width (shortest dimension) (12, 13).

Ultrasound measurements. Ultrasound measurements were conducted at 1, 2, 3, 4, 5, 6, 8, 10, 12, 14 and 16 weeks prior to sacrificing the animals. Mice were scanned with a 14-MHz transducer (Acuson Sequoia ultrasound, Siemens, Malvern, PA, USA) and images were obtained in transverse and sagittal planes. In addition to size measurements, spectral Doppler was employed to document blood flow within the tumor tissue.

Ascites and analysis of metastasis. Twelve weeks after implantation, ascites was collected prior to surgical tumor harvest. Any remaining ascites after harvesting tumors was combined with the ascites collected prior to surgery to assess the total amount of ascites produced from each animal as accurately as possible. Metastatic lesions were visually confirmed in various organs at 12, 14, and 16 weeks post-exposure and quantified during surgery.

Evaluation of microvessel density. To evaluate microvessel density in tumor tissues, counterstains for both (CD31) and hematoxylin were performed on a representative section of tumor from each time point by ARUP laboratory (ARUP, Salt Lake City, UT, USA). Digital images were acquired by microscopy (Olympus BH-2; Olympus America Inc., Center Valley, PA, USA). The percentage of area stained positively for CD31was analyzed using ImageJ 1.44o software (N.I.H., Bethesda, MD, USA) and a minimum of five high power (×400) fields of view were evaluated for each tissue.

Statistical analysis. Statistical analysis and plotting of graphs were performed using GraphPad Prism software (GraphPad Software Inc., San Diego, CA, USA). All of the results are expressed as the mean±SD, and $p<0.05$ was used for significance.

Results

Establishment of orthotopic mouse ovarian surface epithelial (MOSE) tumors in immune competent C57BL/6 mice. Following orthotopic ID8 cell injections (Figure 1A), we observed tumor formation in the ovary within the first four weeks. After eight weeks, there was significant tumor growth in the left ovary compared to the contralateral ovary (Figure 1B). By 16 weeks, primary tumor weight increased by up to 12-fold and the calculated tumor volume increased 7-fold compared to the control group (Figure 1C and D).

Feasibility of monitoring tumor progression non-invasively by ultrasound. We were able to confirm not only the presence of tumors (Figure 2A, top) but also to document variations in intra-tumoral blood flow and in surrounding tumor tissues at multiple time points during tumorigenesis (Figure 2A, bottom). When comparing tumor volumes calculated from tumors harvested surgically and volumes calculated based upon ultrasound measurements, concordant tumor growth patterns were demonstrated (Figure 2B).

Ascites formation in immune-competent C57BL/6 mice with orthotopic, ovarian ID8 tumors. We observed an increase in abdominal circumference of animals, which was most significant at 12 weeks after ID8 cell implantation. A maximum 11 ml of ascites was drained from one mouse (Figure 3A left and 3D). Comparing changes in body weight and abdominal circumference in animals bearing orthotopic ID8 tumors to those of non-tumor bearing controls, a correlation of ascites formation with tumor progression was noted (Figure 3B-D).

Formation of metastases in orthotopic, ovarian ID8 tumor-bearing mice. As shown in Figure 4A, metastatic lesions on the surface of various organs, including the liver, bowel, stomach, peritoneum, and spleen, as well as tumor implants found on the contralateral saline-injected right ovary were noted. Furthermore, multiple metastatic lesions were observed in various organs such as liver and intestine after 12 weeks of tumor growth periods (Figure 4B).

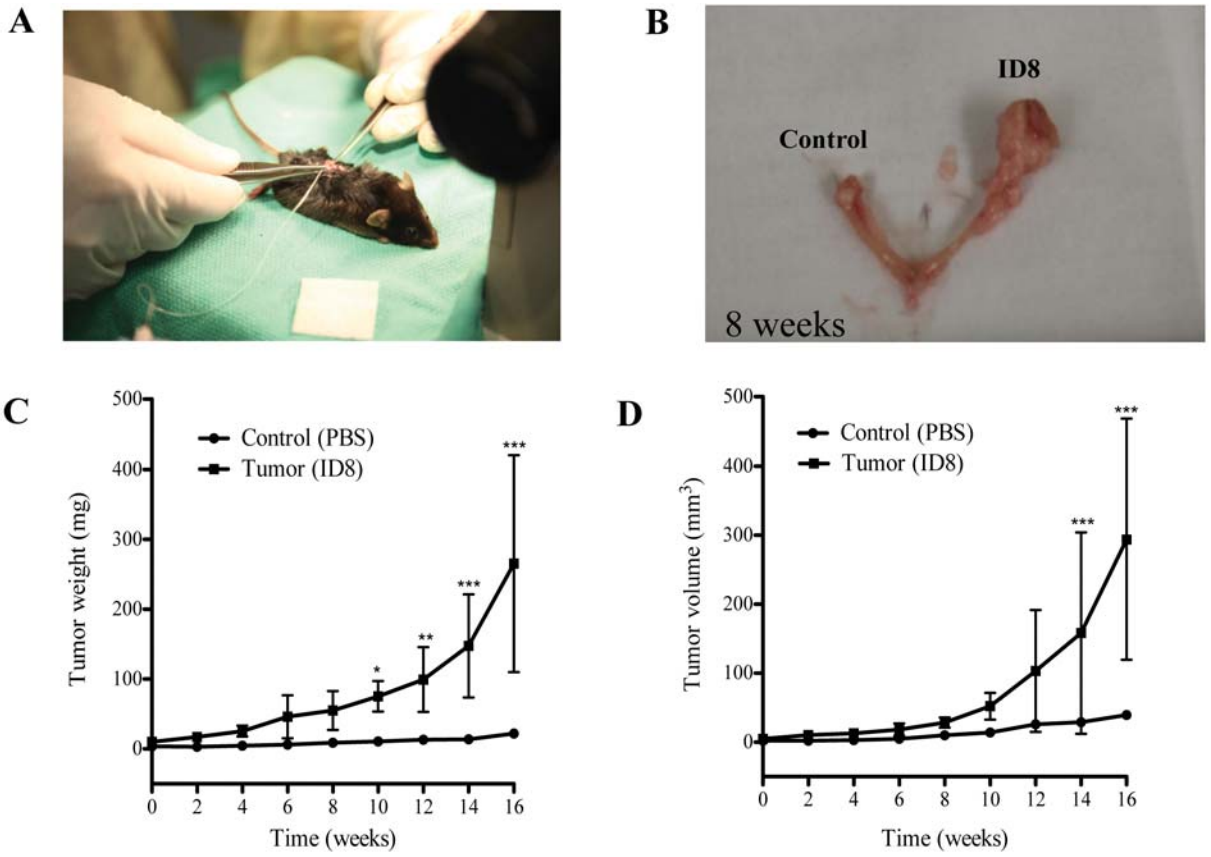

Figure 1. *Establishment of orthotopic mouse ovarian surface epithelial tumors (MOSE-T) in immunocompetent C57BL/6 mice. A: Surgical inoculation of ID8 cells into the left ovarian bursa of C57BL/6 mice. B. Formation of MOSE-T at eight weeks after orthotopic ID8 cell inoculation. C: Time-dependent weight changes of orthotopic MOSE-T in mice. D. Time-dependent volume changes of orthotopic MOSE-T in mice. Data are presented as the mean±S.D. (n=5), *p<0.05, **p<0.01, ***p<0.001. ANOVA test was performed with Bonfferoni post-tests using the GraphPad Prism software.*

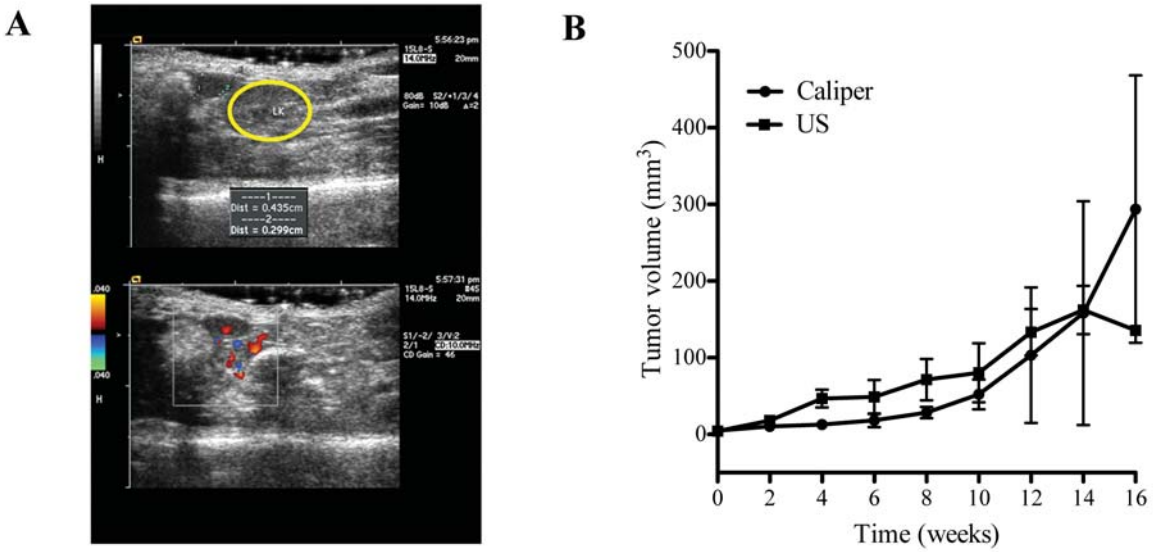

Figure 2. *Comparison of tumor volumes measured either manually (caliper) or using non-invasive ultrasound (US). A: Representative ultrasound image indicating ovarian tumor location (top) and tumor blood flow (bottom). B: Comparison of time-dependent tumor volume changes measured either manually (caliper) or using non-invasive ultrasound (US).*

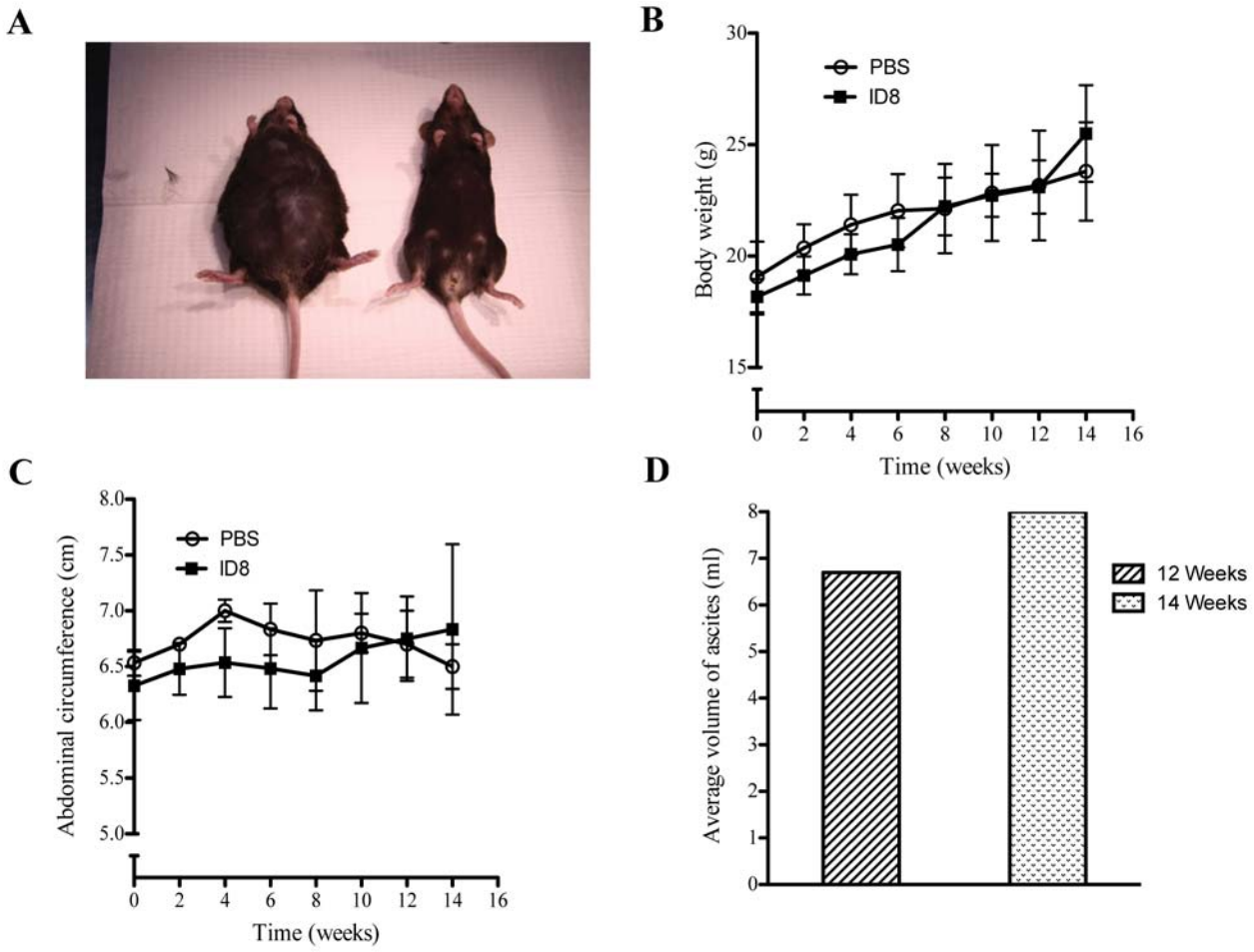

Figure 3. *Ascites formation in immunocompetent C57B/6 mice with orthotopic (MOSE-T). A: Representative image of an ID8 tumor-bearing mouse with ascites formation (animal on the left) and non-tumor bearing, PBS-injected mouse (animal on the right). B and C: Time-dependent changes of body weight and abdominal circumference of tumor-bearing and non-tumor bearing mice. D: Ascites samples collected from mice after 12 and 14 weeks tumor growth.*

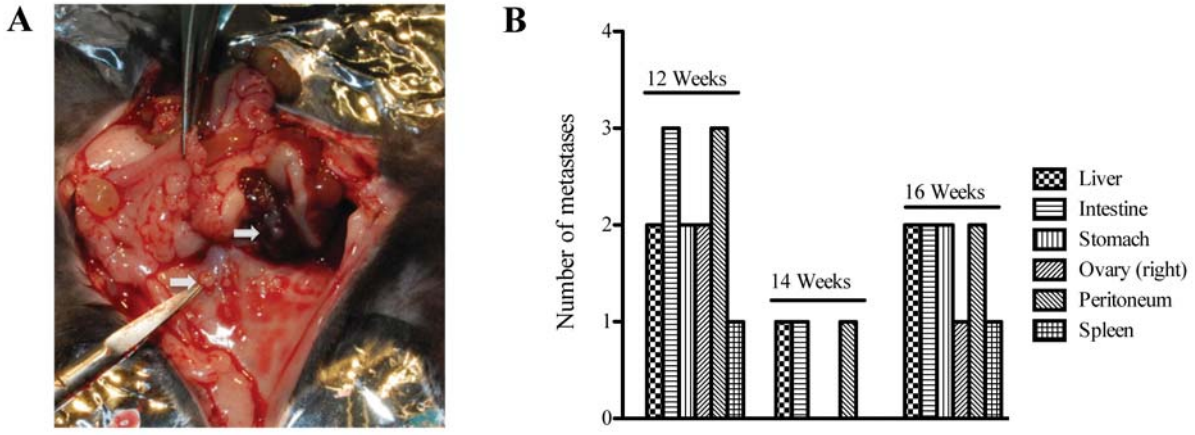

Figure 4. *Metastases of orthotopic (MOSE-T). A: Observation of metastatic lesions on liver and omentum 12 weeks after orthotopic ID8 cell inoculation. B: Quantification and location of metastases.*

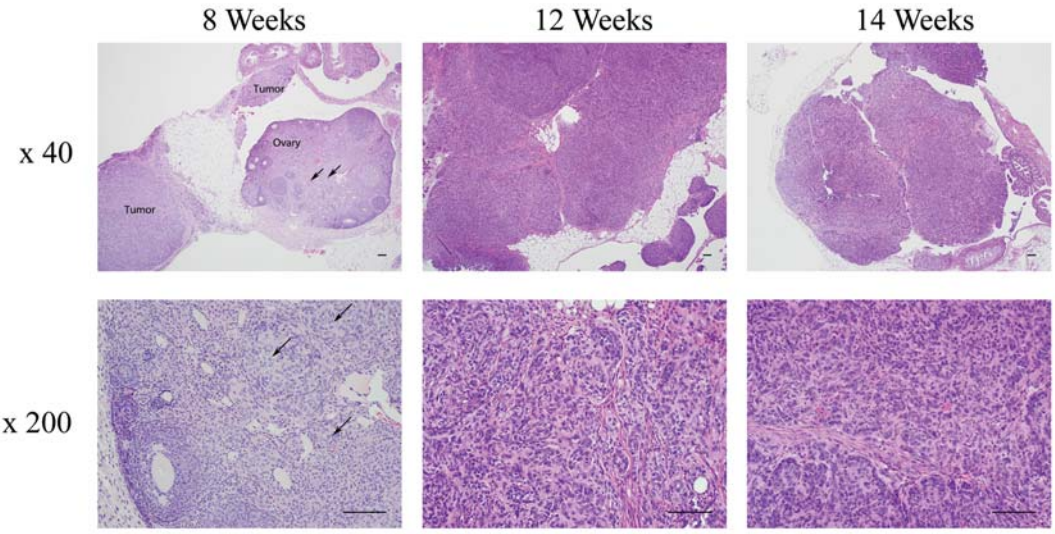

Figure 5. *Histopathology of (MOSE-T) at various time points. Arrows indicate ovarian parenchyma. Hematoxylin and eosin stain; scale bar=100 μm.*

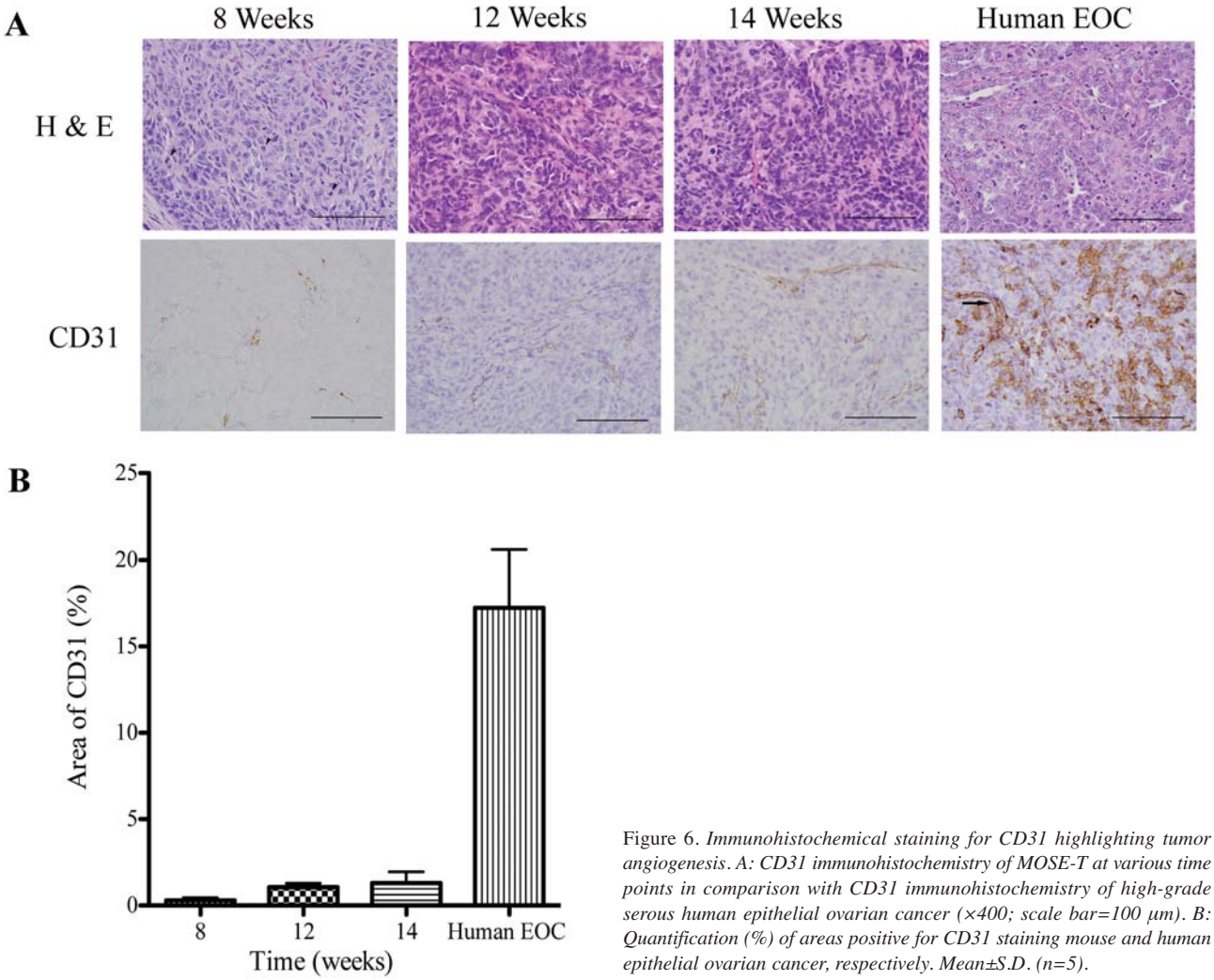

Figure 6. *Immunohistochemical staining for CD31 highlighting tumor angiogenesis. A: CD31 immunohistochemistry of MOSE-T at various time points in comparison with CD31 immunohistochemistry of high-grade serous human epithelial ovarian cancer (×400; scale bar=100 μm). B: Quantification (%) of areas positive for CD31 staining mouse and human epithelial ovarian cancer, respectively. Mean±S.D. (n=5).*

Histopathological studies of orthotopic, ovarian ID8 tumors. At eight weeks, large primary tumor nodules were confined to the bursa and to the periovarian soft tissue. Additionally, isolated nests of tumor cells focally infiltrated into the ovarian parenchyma (Figure 5). At 12 weeks, large nodules of tumor had completely replaced the normal ovary and extensively involved the periovarian soft tissue (Figure 5). At an advanced stage of tumor growth (14 weeks), ID8 orthotopic tumors consisted of large nodules of tumor, completely replacing structures of the normal ovary and also periovarian soft tissues, with variably-sized nests of tumor cells replacing the ovarian parenchyma (Figure 5). The cytological features of the tumor cells themselves were the same at all time points; the cells were morphologically characteristic of an epithelial malignancy and exhibited moderate to marked atypia, with high nuclear to cytoplasmic ratios, oval to round nuclei with coarse chromatin and variably conspicuous nucleoli, as well as brisk mitotic activity.

Immunohistochemical analysis of blood vessel formation and density. To address questions of whether this ID8 orthotopic, ovarian model replicates the angiogenic aspects of ovarian cancer, we performed H&E staining and immunohistochemical staining with antibodies directed against CD31. CD31 is a key molecular marker widely used in experimental studies to quantify tumor neovascularization in terms of vessel density in animal models (14). Furthermore, we also compared the development of angiogenic vessels within advanced-stage ID8 tumors to advanced human ovarian cancer. Orthotopic ID8 tumor tissues consistently exhibited increase in most of the angiogenic vessels from eight weeks up to 14 weeks of tumor growth (Figure 6A and B). However, the development of angiogenic vessels in orthotopic ID8 tumor tissues at 14 weeks, which can be compared to advanced stages of human EOC, was significantly lower than that found in similarly advanced human EOC tissues (Figure 6A), demonstrating that the percentage area of CD31 stains was 1.3±0.7% in ID8 at 14 weeks and 17.2±3.4% in advanced human EOC (Figure 6B).

Discussion

A recent humanized ovarian mouse model through intraperitoneal implantation demonstrated some clinical resemblance to human ovarian cancer, with ascites and metastases (15). However, intraperitoneal implantation of ovarian cancer cells has limitations in replicating critical tumor and stromal interactions and has provided only an indirect understanding of potential disease development and progression (16). Based on a previous report by Greenway *et al*., who established a syngeneic, orthotopic EOC animal model suggesting a potential solution to overcome the limitations of intraperitoneal implantation (5), we further characterized the unknown details of tumorigenesis in this model to identify translational barriers leading to major discrepancies between pre-clinical and clinical outcomes. Our orthotopic model demonstrated the successful formation of primary epithelial ovarian tumors within the ovarian environment as well as the development of secondary, metastatic intraperitoneal lesions. After twelve to fourteen weeks of tumor growth the formation of extensive abdominal ascites was noted. Tumor-bearing animals became moribund and their lower body weights compared to healthy, non-tumor-bearing controls could be explained due to disease progression. Differences in body weight and abdominal circumferences were not statistically significant. Morphological features reflect the disease progression observed in human EOC.

Current monitoring of tumor progression in primary orthotopic ovarian lesions is limited by the need to sacrifice the animal to harvest and assess tumors. This methodology is costly and highly inefficient (17). Non-invasive methods of monitoring tumor progression have focused on applying various imaging technologies, such as ultrasound, contrast agent-based positron-emission tomography (PET), magnetic resonance imaging (MRI), and optical imaging, encompassing bioluminescence imaging (BLI) and fluorescence imaging (FLI) (18). In this study, we explored transabdominal ultrasound as a potentially cost-effective method to monitor EOC tumors. Ultrasound proved to be successful in monitoring blood flow alterations associated with tumorigenesis. Primary tumors were detectable as early as three weeks post-implantation. Tumor volumes obtained by manual digital caliper measurements and ultrasonic measurements yielded nearly identical tumor growth patterns. Considering the convenience, accessibility, lower cost, reduced animal requirements and consistent reproducibility, ultrasound assessment of tumor growth and metastasis should be further explored.

Around 12 weeks post-implantation of ID8 cells, mice developed ascites, replicating human disease (5). Increased levels of vascular endothelial growth factor (VEGF) in the primary and secondary tumors may play a key role in ascites formation *via* increased vascular permeability and enhanced leakiness of blood vessels (19, 20). Based on tumor cell behavior, two ascite variants, stimulatory or inhibitory, impact the cellular and molecular parameters of ovarian cancer (21). In our EOC model the formation of ascites was associated with increased tumor volumes as well as the formation of metastatic lesions.

Due to a limited supply of nutrients and oxygen in many types of solid tumors, angiogenesis is an essential requisite of growth and metastasis (22). Therefore, angiogenesis is a

hallmark of tumor growth and metastasis, and a promising therapeutic target. In addition to directly inhibiting angiogenesis, utilizing the leaky architecture to achieve enhanced permeability and retention (EPR) of anticancer agents may demonstrate additional potency. Thus far, EPR has only shown its potential contribution to the accumulation of anticancer drugs being nanoparticles or liposomes in animal models. Furthermore, the tumor's increased interstitial fluid pressure of tumor may inhibit drug delivery by counteracting deeper tumor penetration (22-25). Increased understanding of the angiogeneic properties of this tumor model will help in the exploration of numerous interventional strategies. This orthotopic animal model demonstrated the gradual increase of angiogenic vasculature during the period of tumor growth. However, when compared to the angiogenic vasculature in human EOC tissues, a significantly lower volume of such vessels was observed in the animal tumors. This apparent difference could limit the application of this animal model when attempting to estimate antiangiogenic effects of drugs or EPR-based drug delivery systems and also serve as an explanation as to why discrepancies occur between pre-clinical animal model data and clinical studies (26). Although each animal model has limitations, we believe that orthotopic ovarian cancer models more closely replicate and may provide a better understanding of the development, progression, metastasis, and angiogenic factors associated with human EOC.

In conclusion, we characterized the development and progression of a syngeneic EOC animal model utilizing the orthotopic implantation of murine ID8 cells in immunocompetent female C57BL/6 mice. This animal model of EOC closely represented characteristics and features of human EOC, including the formation of primary lesions, ascites, and metastases, as well as angiogenesis. Limitations of this animal model regarding angiogenesis have been raised. Furthermore, we demonstrated that ultrasound can be used successfully to monitor disease progression. Continued evaluation of the role of ascites, tumor microenvironment, development of drug resistance and existence and role of cancer stem cells are required to understand the complex interactions of ascites within the peritoneum and the various organs that may influence EOC progression, metastasis and recurrence.

Acknowledgements

We thank ARUP laboratories, especially Ms. Sheryl Tripp for her kind support performing histopathological staining and Dr. Anna Baker for her logistic support conducting the animal experiments. This research was supported in part by an NIH research grant (R01-CA140348) and by a Seed grant from the University of Utah, as well as the Department of Obstetrics and Gynecology at the University of Utah.

References

1 Siegel R, Naishadham D and Jemal A: Cancer statistics, 2012. CA Cancer J Clin *62*: 10-29, 2012.
2 American Cancer Society (ACS): Cancer Facts & Figures 2010. American Cancer Society:1-66, 2010.
3 Jelovac D and Armstrong DK: Recent progress in the diagnosis and treatment of ovarian cancer. CA Cancer J Clin *61*: 183-203, 2010.
4 Landen CN Jr., Birrer MJ and Sood AK: Early events in the pathogenesis of epithelial ovarian cancer. J Clin Oncol *26*: 995-1005, 2008.
5 Greenaway J, Moorehead R, Shaw P, and Petrik J: Epithelial–stromal interaction increases cell proliferation, survival and tumorigenicity in a mouse model of human epithelial ovarian cancer. Gynecol Oncol *108*: 385-394, 2008.
6 Shaw TJ, Senterman MK, Dawson K, Crane CA and Vanderhyden BC: Characterization of intraperitoneal, orthotopic, and metastatic xenograft models of human ovarian cancer. Mol Ther *10*: 1032-1042, 2004.
7 Connolly DC and Hensley HH: Xenograft and transgenic mouse models of epithelial ovarian cancer and non-invasive imaging modalities to monitor ovarian tumor growth *in situ*-applications in evaluating novel therapeutic agents. Curr Protoc Pharmacol *45*: 14.12. 11-14.12.26, 2009.
8 Connolly DC, Bao R, Nikitin AY, Stephens KC, Poole TW, Hua X, Harris SS, Vanderhyden BC and Hamilton TC: Female mice chimeric for expression of the simian virus 40 TAg under control of the *MISIIR* promoter develop epithelial ovarian cancer. Cancer Res *63*: 1389-1397, 2003.
9 Jacobs AJ, Curtis GL, Newland JR, Wilson RB and Ryan WL: Chemical induction of ovarian epithelial carcinoma in mice. Gynecol Oncol *18*: 177-180, 1984.
10 Nishida T, Sugiyama T, Kataoka A, Ushijima K and Yakushiji M: Histologic characterization of rat ovarian carcinoma induced by intraovarian insertion of a 7,12-dimethylbenz[a]anthracene-coated suture: Common epithelial tumors of the ovary in rats? Cancer *83*: 965-970, 1998.
11 Bast RC Jr., Hennessy B and Mills GB: The biology of ovarian cancer: New opportunities for translation. Nat Rev Cancer *9*: 415-428, 2009.
12 Zhang L, Yang N, Garcia JR, Mohamed A, Benencia F, Rubin SC, Allman D and Coukos G: Generation of a syngeneic mouse model to study the effects of vascular endothelial growth factor in ovarian carcinoma. Am J Pathol *161*: 2295-2309, 2002.
13 Tomayko MM and Reynolds CP: Determination of subcutaneous tumor size in athymic (nude) mice. Cancer Chemother Pharmacol *24*: 148-154, 1989.
14 Wang D, Stockard CR, Harkins L, Lott P, Salih C, Yuan K, Buchsbaum D, Hashim A, Zayzafoon M, Hardy RW, Hameed O, Grizzle W and Siegal GP: Immunohistochemistry in the evaluation of neovascularization in tumor xenografts. Biotech Histochem *83*: 179-189, 2008.
15 Bankert RB, Balu-Iyer SV, Odunsi K, Shultz LD, Kelleher RJ, Jr., Barnas JL, Simpson-Abelson M, Parsons R and Yokota SJ: Humanized mouse model of ovarian cancer recapitulates patient solid tumor progression, ascites formation, and metastasis. PLoS One *6*: e24420, 2011.
16 Thaker PH, Han LY, Kamat AA, Arevalo JM, Takahashi R, Lu C, Jennings NB, Armaiz-Pena G, Bankson JA, Ravoori M,

Merritt WM, Lin YG, Mangala LS, Kim TJ, Coleman RL, Landen CN, Li Y, Felix E, Sanguino AM, Newman RA, Lloyd M, Gershenson DM, Kundra V, Lopez-Berestein G, Lutgendorf SK, Cole SW and Sood AK: Chronic stress promotes tumor growth and angiogenesis in a mouse model of ovarian carcinoma. Nat Med *12*: 939-944, 2006.

17 Lyons SK: Advances in imaging mouse tumour models *in vivo*. J Pathol *205*: 194-205, 2005.

18 Fanelli M, Locopo N, Gattuso D and Gasparini G: Assessment of tumor vascularization: immunohistochemical and non-invasive methods. Int J Biol Markers *14*: 218-231, 1999.

19 Hicklin DJ and Ellis LM: Role of the vascular endothelial growth factor pathway in tumor growth and angiogenesis. J Clin Oncol *23*: 1011-1027, 2005.

20 Hu L, Ferrara N and Jaffe RB: Paracrine VEGF/VE-cadherin action on ovarian cancer permeability. Exp Biol Med *231*: 1646-1652, 2006.

21 Puiffe ML, Le Page C, Filali-Mouhim A, Zietarska M, Ouellet V, Tonin PN, Chevrette M, Provencher DM and Mes-Masson AM: Characterization of ovarian cancer ascites on cell invasion, proliferation, spheroid formation, and gene expression in an in vitro model of epithelial ovarian cancer. Neoplasia *9*: 820-829, 2007.

22 Burger RA: Experience with bevacizumab in the management of epithelial ovarian cancer. J Clin Oncol *25*: 2902-2908, 2007.

23 Chauhan VP, Stylianopoulos T, Martin JD, Popovic Z, Chen O, Kamoun WS, Bawendi MG, Fukumura D, and Jain RK: Normalization of tumour blood vessels improves the delivery of nanomedicines in a size-dependent manner. Nat Nanotechnol *7*: 383-388, 2012.

24 Matsumura Y and Maeda H: A new concept for macromolecular therapeutics in cancer chemotherapy: Mechanism of tumoritropic accumulation of proteins and the antitumor agent smancs. Cancer Res *46*: 6387-6392, 1986.

25 Nagy JA, Meyers MS, Masse EM, Herzberg KT and Dvorak HF: Pathogenesis of ascites tumor growth: Fibrinogen influx and fibrin accumulation in tissues lining the peritoneal cavity. Cancer Res *55*: 369-375, 1995.

26 Shanks N, Greek R and Greek J: Are animal models predictive for humans? Philos Ethics Humanit Med *4*: 2, 2009.

Received February 19, 2013
Revised March 18, 2013
Accepted March 19, 2013